Long-lasting goodshielding at the equatorial ionosphere

Yong Wei,[1,2] Zuyin Pu,[2] Minghua Hong,[1] Qiugang Zong,[2] Jianjun Liu,[3] Jianpeng Guo,[4] Aaron Ridley,[5] and Weixing Wan[1]

Received 7 June 2010; revised 3 September 2010; accepted 8 September 2010; published 30 December 2010.

[1] During magnetic storm times, a dawnward electric field may build up at the Alfven layer in the inner magnetosphere to cancel an enhanced duskward magnetospheric convection electric field. This effect is known as "shielding" because the dawnward electric field prevents the duskward electric field from penetrating into the inner magnetosphere. The term "goodshielding" refers to the perfect shielding status, in which the penetration electric field is almost completely canceled by shielding electric field. Observational evidence of goodshielding has rarely been reported before. Here we present two long-lasting (16 and 23 min) goodshielding cases as unambiguous evidence. Both cases show similar historical patterns of shielding status: long-duration electric field penetration (undershielding), goodshielding, and then overshielding. The goodshielding time periods, featuring quiet-level ionospheric electric field at the dayside equator, are not directly related to the changes of interplanetary magnetic field (IMF) B_Z, but the transitions from goodshielding to overshielding coincide with reduction of convection electric field. Both cases show that the equatorial electric field does not significantly respond to convection electric field enhancements during goodshielding, indicating that the shielding electric field may quickly adjust to shield newly enhanced convection electric fields. The quick shielding is possibly attributed to the fact that the ring current has become stronger and has been brought closer to the Earth. These new features may provide some clues to understand the magnetosphere-ionosphere coupling processes during storm times.

Citation: Wei, Y., Z. Pu, M. Hong, Q. Zong, J. Liu, J. Guo, A. Ridley, and W. Wan (2010), Long-lasting goodshielding at the equatorial ionosphere, *J. Geophys. Res.*, *115*, A12256, doi:10.1029/2010JA015786.

1. Introduction

[2] To understand the transformation of solar wind energy input into the Earth's magnetosphere-ionosphere system, significant effort has been devoted to investigating the dynamics of the magnetosphere during storm times when southward interplanetary magnetic field (IMF) B_Z opens a channel to convey solar wind energy through dayside magnetic reconnection. An important process is that the large-scale earthward plasma convection in the magnetotail is typically prevented from crossing the Alfven layer, which means it cannot penetrate into the inner magnetosphere. If we describe it with the electric field and current [*Vasyliūnas*, 2001], this process can be understood as the convection electric field being prevented from penetrating inside. It is already known that the charge accumulation at the Alfven layer/ring current region can build up a dawnward electric field to cancel duskward convection electric field, thus the inner magnetosphere is shielded by this dawnward shielding electric field [*Wolf et al.*, 2007].

[3] However, the shielding effect seems to be not always effective. Since the charge accumulation at the Alfven layer usually takes time to increase to reach an effective level, the inner magnetosphere is typically disturbed by the penetrating electric field during the first several tens of minutes to several hours [*Huang et al.*, 2005]. Furthermore, this penetrating electric field maps into the midlatitude and low-latitude ionosphere along magnetic field lines, causing ionospheric and geomagnetic disturbances [*Kelley*, 1989; *Fejer*, 2002].

[4] The present in situ observations made by spacecrafts cannot provide enough information for studying large-scale shielding electric fields at the Alfven layer, thus the ionospheric and geomagnetic responses are usually used to infer the shielding status. *Nishida* [1968] first noticed that the geomagnetic DP2 fluctuations are coherent with the variations in the north-south component of the interplanetary magnetic field (IMF), and further, he suggested that the penetration of the interplanetary electric field (IEF) into the magnetosphere is the origin of the DP2 variations, which can reach to the equatorial ionosphere. On the basis of comprehensive data, *Kikuchi et al.* [1996] described more details on the relationship between DP2 fluctuations and penetration electric fields. In recent years, the equatorial ionospheric

[1]Beijing National Observatory of Space Environment, Institute of Geology and Geophysics, Chinese Academy of Sciences, Beijing, China.
[2]School of Earth and Space Sciences, Peking University, Beijing, China.
[3]Polar Research Institute of China, Shanghai, China.
[4]State Key Laboratory of Space Weather (Center for Space Science and Applied Research, Chinese Academy of Sciences), Beijing, China.
[5]Department of Atmospheric, Oceanic, and Space Sciences, University of Michigan, Ann Arbor, Michigan, USA.

0148-0227/10/2010JA015786

electric field data measured by the Jicamarca Incoherent Scatter Radar (ISR) provide unambiguous evidence for the penetration scenario [e.g., *Fejer and Scherliess*, 1997; *Kelley et al.*, 2003; *Huang et al.*, 2005; *Wei et al.*, 2008a; *Guo et al.*, 2010]. This electric field penetration phenomenon is alternatively called "undershielding," which means that the shielding electric field is weaker than the convection electric field. Quite recently, the undershielding has again been shown to be crucial when interpreting some interesting ionospheric disturbances [e.g., *Huang*, 2009; *Li et al.*, 2009, 2010; *Zong et al.*, 2010].

[5] In the opposite case, the shielding electric field can be stronger than the convection electric field, which is typically referred to as "overshielding" [*Kelley et al.*, 1979]. The IMAGE satellite provided clear evidence for overshielding through the confirmation of the theoretically predicted "shoulder" structure in the plasmasphere [*Goldstein et al.*, 2002, 2003]. The typical IMF condition for overshielding is an abrupt northward turning after prolonged southward IMF, because in the inner magnetosphere it still needs time to remove the accumulated charges after the convection electric field suddenly drops with the northward turning [e.g., *Ebihara et al.*, 2008]. Note that the "northward turning" is also referred to as a decrease of southward IMF, where the IMF does not become northward [*Kikuchi et al.*, 2008]. On the other hand, *Fejer et al.* [1990] proposed that the changes of magnetospheric configuration also affect shielding process. This idea was recently confirmed by the observations of an overshielding case [*Wei et al.*, 2008b] and was used to interpret westward electric fields on the dayside equatorial ionosphere during a substorm [*Wei et al.*, 2009]. We emphasize that the overshielding effect must appear after undershielding if it indeed happens.

[6] Theoretically, there should be a "goodshielding" status, i.e., the shielding electric field is approximately equivalent to the convection electric field [*Goldstein*, 2006; *Wolf et al.*, 2007]. To generate goodshielding, there must be a strong enough nightside-centered partial ring current, and the inner edge of the plasma sheet has to come significantly closer to Earth on the nightside than on the dayside. However, gradient/curvature drift may prevent more energetic plasma sheet ions from coming close enough to Earth to contribute to shielding [*Wolf et al.*, 2007]. These considerations imply that goodshielding cases are not as abundant as undershielding and overshielding cases, but they are important for understanding the behavior of the ring current during storm.

[7] There are some difficulties in present goodshielding studies with both observations and computer simulations. For observations, a natural consideration is that the goodshielding perhaps occurs under long-lasting stably southward IMF which ensures an expected strong shielding electric field. However, the continuous energy input into the magnetosphere may lead to substorm activity which modifies the shielding electric field development [*Huang et al.*, 2004]. Another consideration is that the goodshielding must be embedded in the transition from undershielding to overshielding, but in most of reported cases the transition from undershielding to overshielding is transient [e.g., *Kelley et al.*, 1979]. For such a case, the determination of goodshielding duration is limited by the time resolution of electric field data. Since there is usually only one data point can be classified as goodshielding, the corresponding duration is estimated at less than 10 min for Jicamarca ISR data (resolution 5 min) or 2 min for geomagnetic-inferred data (resolution 1 min). This duration is too short to discern the behavior of magnetosphere-ionosphere system during goodshielding. For computer simulations, there are some uncertainties requiring observational determinations. The Rice Convection Model (RCM) had successfully reproduced and predicted main features of undershielding and overshielding [*Toffoletto et al.*, 2003], but it has difficulties for goodshielding because of lack of observations of some input parameters sensitive to RCM [*Wolf et al.*, 2007]. Therefore, we can neither use observations to conduct simulation work nor use simulation results as a guide to identify goodshielding case. The best way to start a goodshielding study may be to find long-lasting goodshielding events, of which the durations are at least longer than 10 min.

[8] There are two kinds of data that can be used. One is the snapshot of plasmasphere made by the IMAGE satellite. *Spasojevic and Goldstein* [2005] thought that the goodshielding should feature a plasmasphere without "plume" structure, which can distinguish goodshielding from undershielding (with plume) and overshielding (with shoulder). The other one is the inferred equatorial electric field, as done in previous undershielding and overshielding studies [*Anderson et al.*, 2002; *Kelley et al.*, 2003]. The latter one has much more data sets than the former since it is obtained by ground-based stations. We thus choose to take the inferred equatorial electric field as an indicator of shielding status. It is known that the equatorial ionospheric electric field can be inferred from the difference between geomagnetic H components (ΔH) of a pair of stations, of which one is located at the geomagnetic equator and the other one is located off the equator [*Anderson et al.*, 2002]. The two geomagnetic stations in Peru (LT = UT − 5 h), Jicamarca (JIC, 11.9°S, 283.1°E, dip 0.8°N) and Piura (PIU, 5.2°S, 279.4°E, dip 6.8°N), meet the requirement to estimate the ionospheric electric field.

[9] We have examined all JIC-PIU ΔH data available online (http://jro.igp.gob.pe/) from 1999 to present, and found two cases that can be regarded as unambiguous evidence of goodshielding. Since the ΔH-inferred equatorial electric field depends on the equatorial electrojet, both cases were observed on the dayside. The criterion is that there should be three well-defined stages: undershielding, long-lasting transition (>10 min) and overshielding. We assume that the equatorial electric field during goodshielding looks like the quiet level, thus our criterion logically exclude a pattern in which a quiet level interval following an undershielding interval, though we believe in some cases this pattern indeed can be interpreted as goodshielding following undershielding. In section 2, we compare the shielding development with solar wind condition and cross polar cap potential; and in section 3, we discuss some physics implied by the observations.

2. Observations

2.1. 23 May 2002 Event

2.1.1. Solar Wind Conditions and Geomagnetic Responses

[10] Figure 1 shows the solar wind dynamic pressure (P_{SW}) and X component of solar wind velocity (V_X), IMF X com-

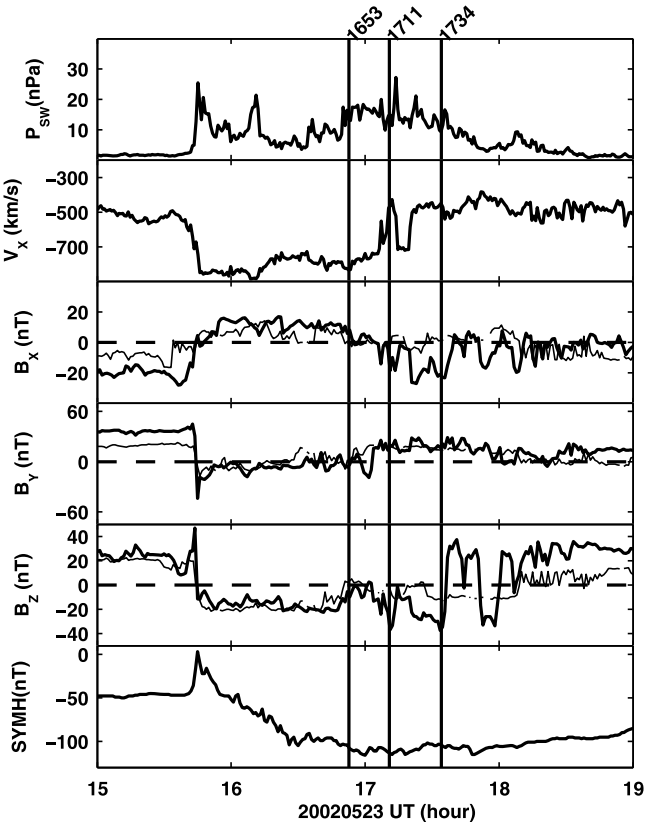

Figure 1. Solar wind conditions and symmetric ring current H index (SYMH) during 1500–1900 UT on 23 May 2002. The observations of solar wind are shown in first through fifth panels: solar wind dynamic pressure (P_{SW}), solar wind speed V_X, IMF X component (B_X), Y component (B_Y) and Z component (B_Z). The thick lines are time-shifted Geotail data, and the thin lines are OMNI data derived from ACE observations at L1 point. The sixth panel is SYMH, which is essentially the same as *Dst* index.

ponent (B_X), Y component (B_Y), Z component (B_Z) and Symmetric ring current H index (SYMH) during 1500–1900 UT on 23 May 2002. The SYMH index is essentially the same as *Dst* but with a 1 min resolution [*Iyemori and Rao*, 1996]. The thick lines are data from Geotail, which was located at (3.2, 21.8, 4.7) R_E in GSM at 1540 UT, while the thin lines are OMNI data derived from ACE observations at the L1 point. The discrepancy between the thick and thin lines suggests that the solar wind has significantly changed during the propagation from ACE to the Earth or there are some small-scale structures in the solar wind. This event started from the recovery phase of the last storm, and the SYMH (~−50 nT) implied a gradually decaying symmetric ring current before the southward turning of IMF B_Z. At 1544 UT, the SYMH suddenly increased, thus we determined 1.2 min time delay for Geotail observations through comparing the dynamic pressure pulse and the SYMH peak, and this time delay has been applied for Figure 1.

[11] The first panel of Figure 2 replots time-shifted Geotail B_Z, and the rest of panels are cross polar cap potential (CPCP), polar cap area (PCA), and JIC-PIU ΔH. The CPCP and PCA are calculated by the Assimilative Mapping of Ionospheric Electrodynamics (AMIE) procedure, which is a technique used to reconstruct the high-latitude ionospheric electrodynamic parameters by combining the various data sets [*Richmond and Kamide*, 1988; *Ridley et al.*, 1998; *Ridley and Kihn*, 2004]. The CPCP can be regarded as a proxy of plasma convection and associated convection electric field, while the PCA is the area of open magnetic field line.

2.1.2. Shielding Status

[12] The shielding status can be identified from JIC-PIU ΔH (fourth panel in Figure 2) according to discussions in section 1. The thick line is the observations on 23 May, while the thin line is the observations on quiet day 24 May as a reference. Please note LT = UT − 5 h. Under northward IMF B_Z (1500–1544 UT), the CPCP was larger than 50 kV and less than 100 kV, and the ΔH was approximately equivalent to quiet level. Because this interval was a part of the recovery phase of last storm, the plasma convection in the polar cap was still active, probably because of the release of previously stored energy in the magnetosphere rather than solar wind

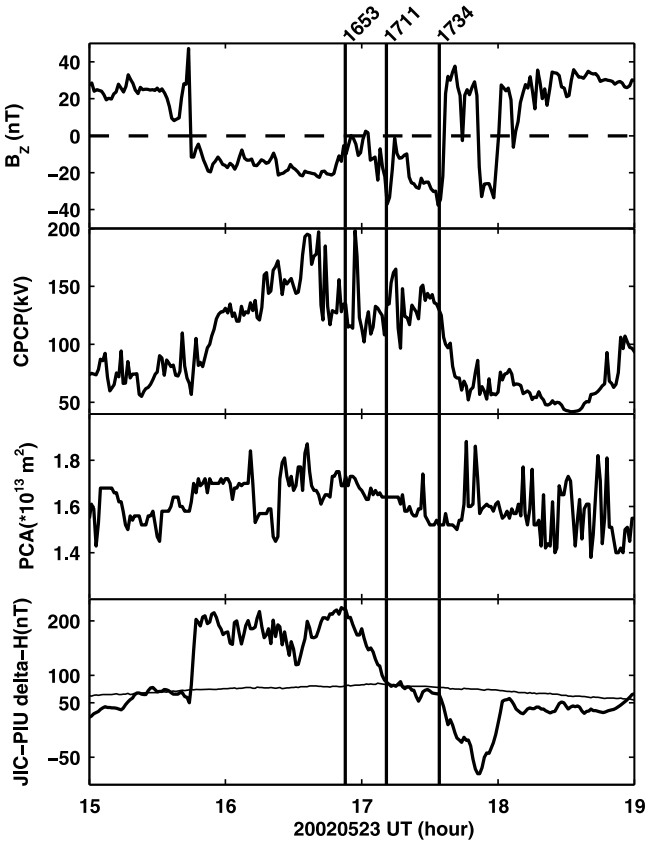

Figure 2. First panel shows replot of IMF B_Z measured by Geotail. Second and third panels show cross polar cap potential (CPCP) and polar cap area (PCA) calculated by the Assimilative Mapping of Ionospheric Electrodynamics (AMIE) procedure. Fourth panel shows JIC-PIU ΔH derived from geomagnetic H component in Jicamarca and Piura stations, which is linearly correlated to equatorial electric field. The positive (negative) corresponds to eastward (westward) electric field. The thick line represents disturbed day, while the thin line is quiet day as a reference; see the text. The goodshielding status appears during 1711–1734 UT.

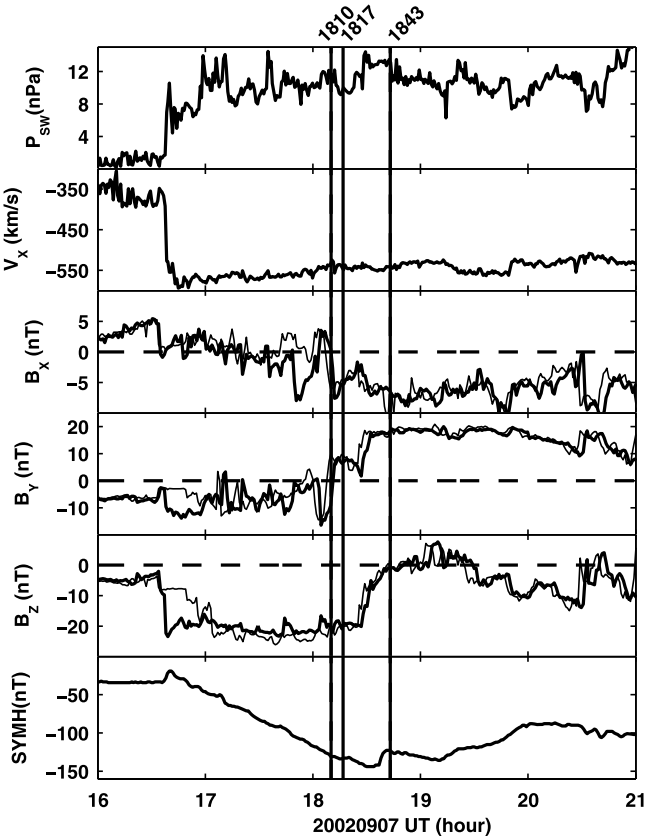

Figure 3. Same parameters as Figure 1 but for 1600–2100 UT on 7 September 2002.

directly driving. After this, there are three time periods of interest.

2.1.2.1. Undershielding (1544–1711 UT)

[13] The ΔH suddenly increased when the IMF B_Z turned southward, indicating the penetration of convection electric fields to the inner magnetosphere. The shielding looks seemingly more effective around 1630 UT (the ΔH decreased), however, the ΔH increased again after 1631 UT, coinciding with CPCP increase from 145 nT to 195 nT. The IMF B_Z started to turn northward at 1648 UT, and the ΔH began to decrease at 1653 UT (the left vertical line) and finally reached the quiet level at 1711 UT. Since the IMF B_Z turned southward again at 1700 UT, we can interpret this ΔH decrease as shielding electric field enhancement instead of convection electric field reduction. The clearest feature can be summarized as: the shielding did not start becoming effective until 1653 UT, and became effective during 1653–1711 UT.

2.1.2.2. Overshielding (1734–1803 UT)

[14] After the IMF B_Z turned to northward at 1734 UT, the CPCP quickly dropped, and the ΔH gradually decreased. The westward equatorial ionospheric electric field during the storm, corresponding to negative ΔH, sometimes can be explained by the disturbance dynamo [*Blanc and Richmond*, 1980]. However, the disturbance dynamo usually takes several hours to become effective and the dynamo continues to work for tens of hours during the geomagnetic storm [*Fejer*, 2002]. Therefore, this ΔH drop from a quiet level within a short time (29 min), associated with IMF B_Z northward turning, was more consistent with overshielding scenario though the contribution of disturbance dynamo may not be completely excluded.

2.1.2.3. Goodshielding (1711–1734 UT)

[15] According to the analysis for undershielding and overshielding, a strong shielding electric field must exist during this interval to produce the followed overshielding feature. Because the ΔH showed a quiet level, we recognized it as a time period of goodshielding status, i.e., the shielding electric field almost completely canceled the convection electric field. This shielding electric field can be confirmed by the enhanced CPCP, in other words, there must be a shielding electric field to cancel the enhanced convection electric field to maintain a quiet-level ΔH. Furthermore, a surprising feature is that the ΔH did not significantly change when both the IMF B_Z and CPCP varied.

2.2. 7 September 2002 Event

2.2.1. Solar Wind Conditions, Geomagnetic and Ionospheric Responses

[16] Figure 3 and Figure 4 are organized as Figure 1 and Figure 2, respectively. Figure 3 shows the P_{SW}, V_X, IMF B_X, IMF B_Y, IMF B_Z and SYMH during 1600–2100 UT on 7 September 2002. The thick lines are Geotail data which were located at (12.2, 21.6, −4.9) R_E in GSM at 1640 UT, while the thin lines are OMNI data derived from ACE

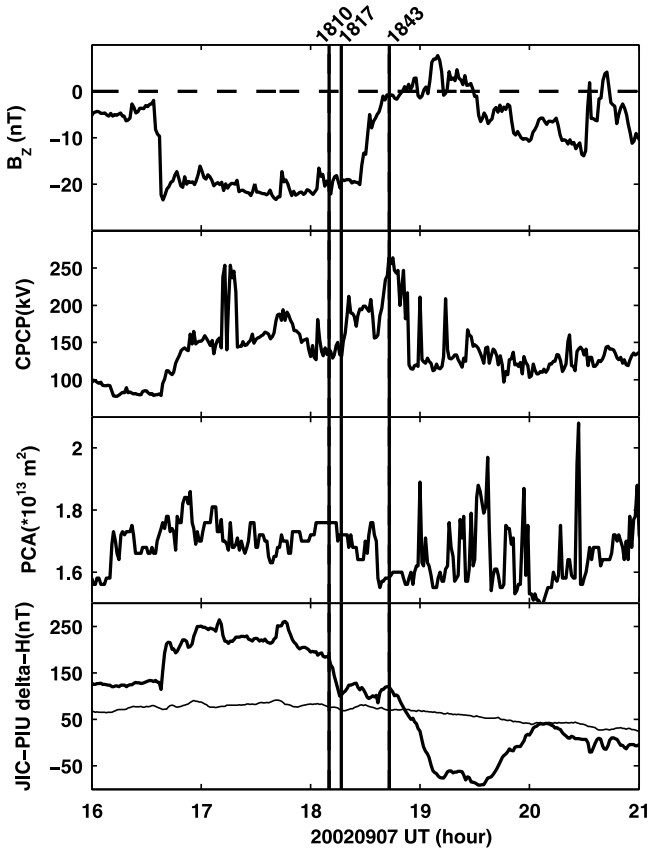

Figure 4. Same parameters as Figure 2 but for 1600–2100 UT on 7 September 2002. The goodshielding status appears during (1817–1843 UT).

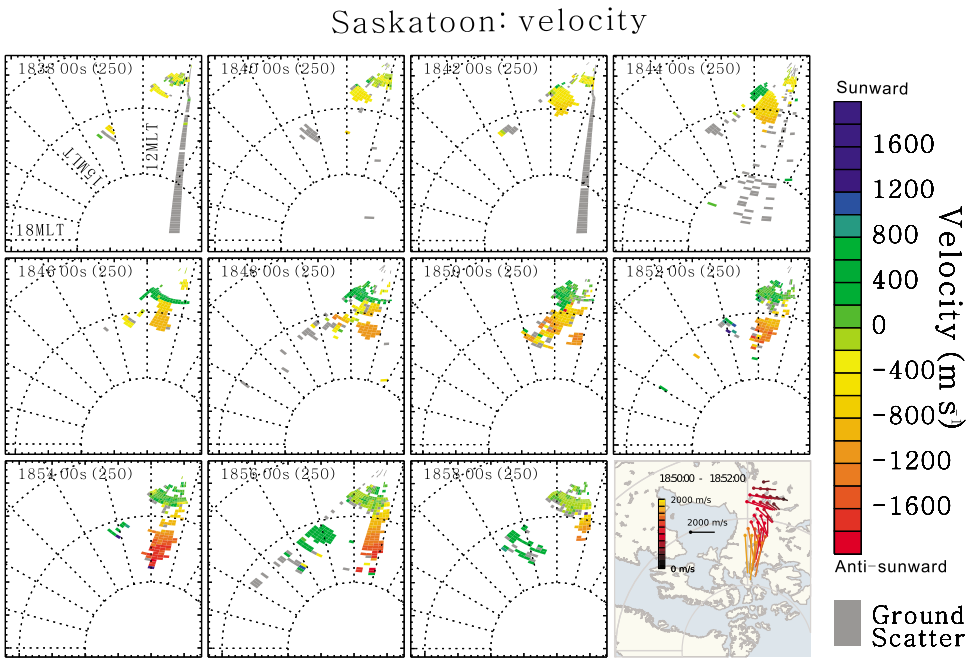

Figure 5. Plasma velocity measured by Saskatoon radar. The right-bottom panel shows convection map for 1850–1852 UT, and the other panels show field of view. The SAS has 16 beams, of which beam 0 (15) is at west (east) of the radar's view, and the view width of each beam is 3.24°. The Sun is on the top. Positive (negative) value means the velocity is toward (away from) SAS radar, and is roughly sunward (antisunward) in our case.

observations at L1 point. The Geotail data have been shifted by 4.8 min, which is determined through match the P_{SW} jump and the Storm Sudden Commencement (SSC) at ~1638 UT in the SYMH. The solar wind and IMF did not significantly change during propagation to the Earth during 1800–1900 UT, the time period of interest in this paper. There was a sharp shock front in original ACE data similar to that observed in the Geotail data (i.e., at 1538 UT), so the deviation of OMNI magnetic field from Geotail around the shock is probably caused by the time shift method for solar wind discontinuities adopted by OMNI. Furthermore, the shift time is slightly underestimated by OMNI. Here we also use Geotail data for this case.

[17] Figure 4 presents IMF B_Z, CPCP, PCA, and JIC-PIU ΔH. Here the reference (thin line) is the ΔH on 8 September. We note that the CPCP enhancement around 1843 UT (the right vertical line), starting at 1838 UT, was not consistent with the pattern of IMF B_Z. To determine whether it was the fact, we checked the observations by Super Dual Auroral Radar Network (SuperDARN).

[18] During 1800–1900 UT, Saskatoon (SAS; GLAT 52.16°N, GLON 106.53°W; MLAT 61.34°N, MLON 45.26°W; LT = UT − 7 h), a member of SuperDARN, was near the local noon (1100–1200 LT). Figure 5 shows "field of view" plot of velocity measured by SAS from 1838 to 1858 UT with 2 min resolution. One of the most striking feature of Figure 5 is the enhanced antisunward flow channel (red color), with a maximum velocity of about 2000 m/s. During 1838–1858 UT, this flow was gradually strengthened from 400 to 2000 m/s. Further, it extended to higher latitude. The right-bottom panel shows the convection map for 1850–1852 UT. Sunward flow (<800 m/s) was also observed but mainly concentrated at lower latitude and was consistent with the throat region. From those snapshots and the convection map, it suggests that the sunward flow was essentially aligned along constant L-shell, maybe because of lobe reconnection and/or return flow of the enhanced antisunward flow.

[19] The SAS observations confirm the CPCP enhancement shown by the AMIE technique. This CPCP enhancement was seemingly caused by B_Y-dominated reconnection (inferred from the fourth panel of Figure 3) or substorm activity (inferred from particle injection observed by LANL, not shown). Discussion of the cause is beyond our goal of this paper.

2.2.2. Shielding Status

[20] Unlike the 23 May 2002 case (case 1), the IMF B_Z was already southward for several hours before the abrupt southward turning at 1635 UT. Thus the discrepancy between the ΔH (thick line) and the reference (thin line) can be caused by electric field penetration and/or day-to-day variability [*Kane*, 1976]. We will discuss this further below. Once again, we discuss three time periods.

2.2.2.1. Undershielding (1635–1817 UT)

[21] The large stable IMF B_Z (~−20 nT) caused significant penetration electric field in the equatorial ionosphere. This interval has been classified as "long-duration penetration" by *Huang et al.* [2005]. The shielding became effective during 1810–1817 UT. This time span (7 min) was shorter than that (18 min) of case 1, indicating that the shielding electric field developed more quickly. We would emphasize that this effective shielding was not triggered by IMF northward

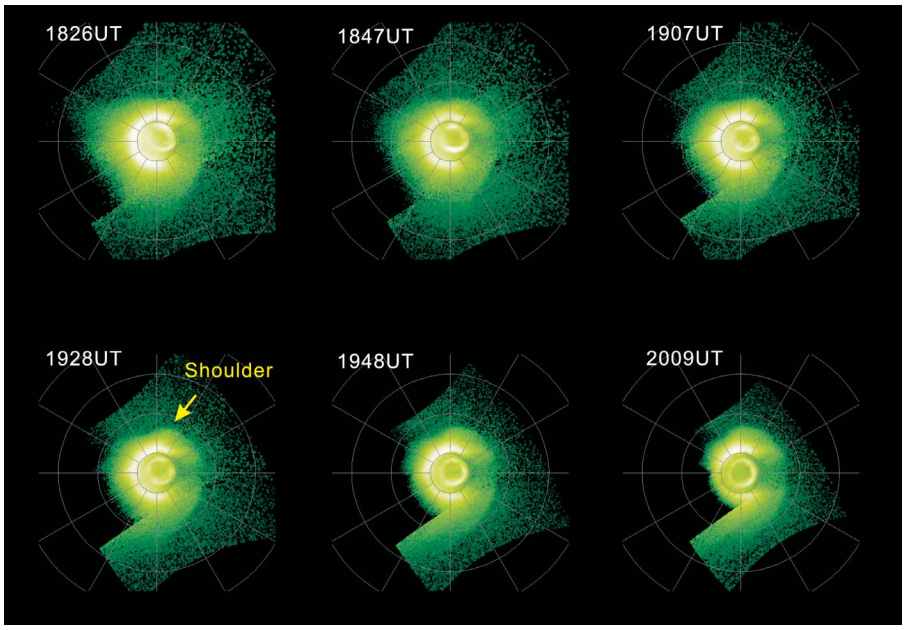

Figure 6. The snapshots of plasmasphere by IMAGE EUV at 1826 UT, 1847 UT, 1907 UT, 1928 UT, 1948 UT, and 2009 UT. Sunlight is incident from the lower left; Earth is in the center. The bright inner ring is the auroral oval. The "shoulder" structure is easily discerned as marked by the arrows.

turning, instead, the IMF B_Z maintained a strongly southward field (~−20 nT).

2.2.2.2. Overshielding (1843–2009 UT)

[22] The ΔH decrease triggered by the CPCP drop is similar to case 1, and is more consistent with overshielding rather than disturbance dynamo. Luckily, the IMAGE satellite provided unambiguous evidence for this idea. Figure 6 illustrates the shape of plasmasphere observed by Extreme Ultraviolet imager (EUV) onboard IMAGE satellite [*Sandel et al.*, 2000]. The original EUV data were acquired while IMAGE was close to apogee, looking down upon the north pole of the Earth. The six snapshots illustrate projection to the plane of the magnetic equator at 1826 UT, 1847 UT, 1907 UT, 1928 UT, 1948 UT and 2009 UT, respectively. The plasmapause is assumed to be the sharp edge where the brightness of 30.4 nm He^+ emissions drops drastically. The overshielding electric field caused antisunward flow of the predawn plasma, producing a bulge that rotated eastward, which was the so-called "shoulder" [*Goldstein et al.*, 2002, 2003].

2.2.2.3. Goodshielding (1817–1843 UT)

[23] According to the logical statements for case 1, this interval embedded in the transition from undershielding to overshielding is a time period of goodshielding. Because of the IMAGE satellite position at this time ((3.34, −0.70, 5.66) R_E in GSE), the details of dayside plasmapause in Figure 6 was not perfect. However, the information is enough to say that the shape of plasmasphere during goodshielding (1826 UT in Figure 6) may confirm the idea of *Spasojevic and Goldstein* [2005], i.e., the goodshielding should feature a plasmasphere without "plume" structure. We note that there was still a discrepancy between the ΔH and the reference, thus it looks like day-to-day variability may exist. Therefore, the day-to-day variability might also exist before 1635 UT, as discussed in first paragraph of section 2.2.2.

3. Discussion

[24] The observed undershielding, goodshielding and overshielding can be explained as a balance between Region 1 (R1) and Region 2 (R2) field aligned currents (FACs) [*Wolf et al.*, 2007]. A rapid southward turning of IMF B_Z will cause the R1 FAC to increase immediately, but the R2 FAC will take longer time (tens of minutes to several hours) to balance the enhanced R1 FAC, because the R2 FAC, depending on charge accumulation on the Alfven layer, needs time to increase to produce the goodshielding. In the opposite case, an abrupt northward turning of IMF B_Z after a prolonged southward orientation may cause the R2 FAC to be stronger than the R1 FAC for a while, then the dawnward shielding electric field can penetrate into the inner magnetosphere. On the basis of this scenario, we discuss some interesting features revealed in the two cases presented above.

3.1. Polar Cap Shrinkage

[25] The polar cap area was calculated from the auroral precipitation results [*Ridley and Kihn*, 2004]. One may note there are some spikes in PCA data during 1800–1900 UT in case 1 as shown in Figure 2 and 1900–2000 UT in case 2 as shown in Figure 4, and this implied unreliable PCA results because the PCA may not change so fast. For discussion purpose, the gradual variations of PCA during transition from undershielding to overshielding can be used to infer the rough changes of polar cap area.

[26] In case 1, the gradually decreased PCA implied that the polar cap area shrunk during 1653–1734 UT. In case 2 (7 September 2002 case), except for the peak around

1834 UT, the PCA also decreased. Furthermore, the SAS observations showed that the antisunward flow shifted to high-latitude region, confirming the polar cap shrinkage. When the location of R1 FAC shifted to higher latitude because of the polar cap shrinkage, the midlatitude and low-latitude electric field associated with R1 FAC would decrease because of the geometrical attenuation of penetrated electric field [*Kikuchi and Araki*, 1979]. Subsequently, the shielding effect will be enhanced even if the intensities of R1 and R2 FACs did not change in this process. This scenario had been used to explain the overshielding feature at the equatorial ionosphere [*Ebihara et al.*, 2008].

[27] The polar cap shrinkage also implies the earthward motion of shielding layer/ring current. *Fejer et al.* [1990] discussed the polar cap shrinkage during magnetic quieting period: the reduction of polar cap area corresponds to a decrease of the flux of field lines threading the magnetotail, which then corresponds to a decrease of the cross-tail current intensity; this lead to the magnetotail becoming more dipolar and the shielding layer/ring current moving earthward. A recent RCM simulation has confirmed this scenario [*Sazykin*, 2000; *Garner et al.*, 2004]. However, the polar cap shrinkage observed in our cases occurred under active periods (the CPCP did not decrease) rather than quieting periods. Furthermore, the shielding is more effective when the Alfven layer moved earthward. Therefore, a possible explanation is that the dipolarization associated with substom brought the Alfven layer to the Earth. We have examined the LANL observations and found an energetic particle injection front around 1653 UT for case 1, but no discernable front around 1810 UT in heavily disturbed observations for case 2. In case 2, the IMF B_Y changed from negative to slightly positive at the onset of goodshielding, and to strongly positive at the northward turning. Because B_Y can strongly control the shape and location of the R1 FAC system, the rearrangement of these currents may cause changes of shielding status.

3.2. Transition From Undershielding to Goodshielding

[28] In our cases, the shielding electric field development looks inconsistent with the conventional idea that the shielding electric field gradually increases during penetration period. For case 2, there was almost no shielding for 95 min (1635–1810 UT), and then the shielding became effective in 7 min (1810–1817 UT). For case 1, the electric field penetration without shielding last for 69 min (1544–1653 UT), during which the discernable effective shielding interval was about 10 min (centered at 1630 UT), and the shielding became effective in 18 min (1653–1711 UT). These time periods are more consistent with high-latitude potential changes, than with R2 FAC rearrangement [*Ridley et al.*, 1998].

[29] This long-duration (>30 min) penetration without significant shielding phenomenon was first reported by *Huang et al.* [2005]. In their pioneer paper, they presented several such kinds of cases and noted that all cases occurred during main phase of storm, thus they concluded that the interplanetary electric field can continuously penetrate to the low-latitude ionosphere without shielding for many hours as long as the strengthening of the magnetic activity is going on under storm conditions. The physics of long-duration penetration had been explored with combination of RCM and the coupled thermosphere ionosphere plasmasphere electrodynamics (CTIPe) model by *Maruyama et al.* [2007]. They theoretically confirmed magnetopsehric reconfiguration scenario [*Fejer et al.*, 1990] and conclude that such a long-lasting "undershielding" effect could result from the constant stretching of the magnetotail during the early main phase of the storm, because the constant stretching mostly on the nightside precludes the reestablishment of shielding across the inner magnetosphere. On the basis of coordinated observations, *Wei et al.* [2010] suggested that the sustained solar wind dynamic pressure should also contribute to long-duration penetration, because high dynamic pressure causes stretching of magnetotail. In our cases, the high dynamic pressure and large southward IMF B_Z are expected to produce significant stretching, and this can help to interpret the long-duration penetration.

[30] However, the cessation of long-duration penetration is more complicated. In case 2, the penetration ceased (1810–1817 UT), i.e., the shielding enhanced, during main phase of storm, under stable southward IMF B_Z, and the P_{SW} and CPCP did not significantly change. In section 3.1., we have discussed the possibility that the penetration was diminished by a substorm. If the cessation was triggered by solar wind changes, the polarity transition of IMF B_X and B_Y would be the candidates (Figure 3). Specially, strong IMF B_Y might cause complicated magnetospheric convection pattern deviating from the classical two cell pattern, and thus the magnetospehric configuration [*Tsyganenko and Stern*, 1996] and convection electric field pattern [*Weimer*, 2001] probably changed when B_Y turned to duskward from dawnward. In case 1, the penetration ceased in the middle of B_Z northward turning rather than at the starting point. Except for this, we did not find other candidate trigger in Figure 1. Another interesting feature of case 1 is that the IMF gradually turned southward from zero when the ΔH decreased (1653–1711 UT). It appears that the inner magnetosphere was not affected by the IMF changes during transition from undershielding to goodshielding. What factors can cease the long-duration penetration? What factors control the time of transition from undershielding to goodshielding? To answer these questions, more works need to be done.

3.3. Transition From Goodshielding to Overshielding

[31] The typical IMF pattern to trigger overshielding is "an abrupt northward turning of IMF B_Z after a prolonged southward orientation" [e.g., *Ebihara et al.*, 2008]. Case 1 was roughly consistent with it, but case 2 was not. However, case 2 did not challenge our present knowledge. The overshielding in case 2 started when the CPCP began to decrease, through IMF B_Z had reached zero 16 min (1827–1843 UT) after the northward turning. Thus case 2 suggested that IMF northward turning is not a sufficient condition to trigger overshielding. However, it does not mean that the IMF B_Z is not as important as the IMF B_Y during this transition. Because the overshielding needs preexisted charge accumulations before convection reduction, the southward IMF B_Z is the primary driver for these charge accumulation.

3.4. Quick Shielding During Goodshielding

[32] Goodshielding refers to the electric field balance between the inner and outer magnetosphere during disturbed

time periods. The observations distinguish it from the balance during quiet time. In case 2, it appears that the ΔH somehow responded to the CPCP variations during goodshielding period, but with relatively small magnitude compared to undershielding period. In other words, once the goodshielding is achieved, it will be quicker to cancel newly enhanced convection electric fields.

[33] There are two possible reasons for the quick shielding. First, as found in the simulation work [*Maruyama et al.*, 2007], if the Alfven layer has already been brought close to the Earth because of long duration undershielding, it will take less time to reconfigure to shield than those beginning from quiet time even for the same convection electric field increment; Furthermore, when the ring current has been largely enhanced during the long time period of undershielding, pressure gradients associated with this well-developed hot pressure distribution in the inner magnetosphere are able to shield the low latitudes better, and may also respond more quickly to changes in the strength of the convection. Second, the polar cap shrinkage may play an important role. As discussed in section 3.1, it can suppress the penetration of convection electric field into inner magnetosphere through the geometrical attenuation of penetrated electric field [*Kikuchi and Araki*, 1979] as well as enhance the shielding electric field through the magnetospheric reconfiguration [*Fejer et al.*, 1990; *Sazykin*, 2000].

3.5. Comments on the Relationship Between Shielding Electric Field and Storm

[34] The degree of shielding effectivity depends on the morphology and intensity of storm time ring current. A strong nightside-centered partial ring current can produce strong R2 FAC to ensure effective goodshielding. On the other hand, the shielding electric field may cause the original open trajectories of injected ions with higher energy to change into closed ones, thus playing a role in the formation of the symmetric ring current [*Xie et al.*, 2006]. Furthermore, the ring current couples to the polar ionosphere through R2 FAC, therefore both shielding electric fields and the ring current are modified by polar ionospheric electrodynamics. What has become clear, after many observational studies in the past several decades, is that undershielding and overshielding frequently occur during the main phase and recovery phase of storm, respectively.

[35] Our discovery of long-lasting goodshielding status sheds new light on this issue. The ring current during the transition from the main phase to the recovery phase quickly responds to variations in convection electric field to shield the inner magnetosphere. To understand this kind of behavior of the ring current, the magnetosphere and ionosphere must be treated as a coupled system. Of particular interest is that the slow changes in the magnetospheric magnetic field cannot be ignored.

[36] The shielding electric field may bridge the storm-substorm relationship, which has been hotly debated in recent two decades [e.g., *Iyemori and Rao*, 1996]. It has already known that the shielding electric field is closely related to substorms, though there are some controversies [*Huang*, 2009; *Wei et al.*, 2009]. This relation was also discussed in section 3.1 in this paper. A new linkage between storm and substorm may be built up when we understand how substorms affect shielding electric fields and how shielding electric fields affect the ring current development.

4. Summary and Conclusions

[37] We have analyzed two cases in which the goodshielding signatures are prolonged. These cases provide a zoom-in view of the transient goodshielding embedded in the transition from undershielding to overshielding in the typical cases reported before [e.g., *Kelley et al.*, 1979]. The observations are summarized as follows:

[38] 1. Both cases occurred under sustained high solar wind dynamic pressure and associated with long-lasting large southward IMF B_Z.

[39] 2. The historical pattern of shielding status is a long-duration penetration (undershielding) goodshielding, and then overshielding.

[40] 3. The transitions from goodshielding to overshielding do not coincide with IMF northward turning, but the transitions are associated with reduction of convection electric field.

[41] 4. The goodshielding features quiet-level ionospheric electric field at the dayside equator. The shielding electric field may quickly adjust to shield newly enhanced convection electric field during goodshielding period.

[42] However, the triggers of transition from undershielding to goodshielding remain unclear, and the physics of "quick shielding" during goodshielding is also an open question. To answer these questions, more case studies and computer simulations are required to determine the factors that control the development of shielding electric field and R2 FAC.

[43] **Acknowledgments.** We sincerely thank B. R. Sandel for providing IMAGE EUV figures and valuable suggestions. We thank one referee for thoughtful comments on the physics of quick shielding and other contributions to improve this paper. This work was supported by the NSFC grants (40974095, 40874088, 40831061, 40731056, and 41004072), the KIP Pilot Project (kzcx2-yw-123) of CAS, Postdoctoral Science Foundation funded project and Open Research Program of SOA Key Laboratory for Polar Science (KP2008008). We acknowledge the CDAWeb for access to the OMNI and Geotail data. The SYMH data are provided by the World Data Center for Geomagnetism at Kyoto University. The Jicamarca Radio Observatory is a facility of the Instituto Geofísico del Perú operated with support from the NSF Cooperative Agreement ATM-0432565 through Cornell University.

[44] Robert Lysak thanks the reviewers for their assistance in evaluating this paper.

References

Anderson, D., A. Anghel, K. Yumoto, M. Ishitsuka, and E. Kudeki (2002), Estimating daytime vertical ExB drift velocities in the equatorial *F* region using ground-based magnetometer observations, *Geophys. Res. Lett.*, *29*(12), 1596, doi:10.1029/2001GL014562.

Blanc, M., and A. D. Richmond (1980), The ionospheric disturbance dynamo, *J. Geophys. Res.*, *85*(A4), 1669–1686, doi:10.1029/JA085iA04p01669.

Ebihara, Y., N. Nishitani, T. Kikuchi, T. Ogawa, K. Hosokawa, and M.-C. Fok (2008), Two-dimensional observations of overshielding during a magnetic storm by the Super Dual Auroral Radar Network (SuperDARN) Hokkaido radar, *J. Geophys. Res.*, *113*, A01213, doi:10.1029/2007JA012641.

Fejer, B. G. (2002), Low latitude storm time ionospheric electrodynamics, *J. Atmos. Sol. Terr. Phys.*, *64*, 1401, doi:10.1016/S1364-6826(02)00103-7.

Fejer, B. G., and L. Scherliess (1997), Empirical models of storm time equatorial zonal electric fields, *J. Geophys. Res.*, *102*(A11), 24,047–24,056, doi:10.1029/97JA02164.

Fejer, B. G., R. W. Spiro, R. A. Wolf, and J. C. Foster (1990), Latitudinal variation of perturbation electric fields during magnetically disturbed

periods: 1986 SUNDIAL observation and model results, *Ann. Geophys.*, *8*, 441–454.

Garner, T. W., R. A. Wolf, R. W. Spiro, W. J. Burke, B. G. Fejer, S. Sazykin, J. L. Roeder, and M. R. Hairston (2004), Magnetospheric electric fields and plasma sheet injection to low L-shells during the 4–5 June 1991 magnetic storm: Comparison between the Rice Convection Model and observations, *J. Geophys. Res.*, *109*, A02214, doi:10.1029/2003JA010208.

Goldstein, J. (2006), Plasmasphere response: Tutorial and review of recent imaging results, *Space Sci. Rev.*, *124*, 203–216, doi:10.1007/s11214-006-9105-y.

Goldstein, J., R. W. Spiro, P. H. Reiff, R. A. Wolf, B. R. Sandel, J. W. Freeman, and R. L. Lambour (2002), IMF-driven overshielding electric field and the origin of the plasmaspheric shoulder of May 24, 2000, *Geophys. Res. Lett.*, *29*(16), 1819, doi:10.1029/2001GL014534.

Goldstein, J., R. W. Spiro, B. R. Sandel, R. A. Wolf, S.-Y. Su, and P. H. Reiff (2003), Overshielding event of 28–29 July 2000, *Geophys. Res. Lett.*, *30*(8), 1421, doi:10.1029/2002GL016644.

Guo, J., et al. (2010), Interplanetary drivers of ionospheric prompt penetration electric fields, *J. Atmos. Sol. Terr. Phys.*, doi:10.1016/j.jastp.2010.01.010, in press.

Huang, C.-S. (2009), Eastward electric field enhancement and geomagnetic positive bay in the dayside low-latitude ionosphere caused by magnetospheric substorms during sawtooth events, *Geophys. Res. Lett.*, *36*, L18102, doi:10.1029/2009GL040287.

Huang, C.-S., J. C. Foster, L. P. Goncharenko, G. D. Reeves, J. L. Chau, K. Yumoto, and K. Kitamura (2004), Variations of low-latitude geomagnetic fields and *Dst* index caused by magnetospheric substorms, *J. Geophys. Res.*, *109*, A05219, doi:10.1029/2003JA010334.

Huang, C.-S., J. C. Foster, and M. C. Kelley (2005), Long-duration penetration of the interplanetary electric field to the low-latitude ionosphere during the main phase of magnetic storms, *J. Geophys. Res.*, *110*, A11309, doi:10.1029/2005JA011202.

Iyemori, T., and D. R. K. Rao (1996), Decay of the *Dst* field of geomagnetic disturbance after substorm onset and its implication on storm-substorm relation, *Ann. Geophys.*, *14*, 608–618, doi:10.1007/s00585-996-0608-3.

Kane, R. P. (1976), Geomagnetic field variations, *Space Sci. Rev.*, *18*, 413–540, doi:10.1007/BF00217344.

Kelley, M. C. (1989), *The Earth's Ionosphere Plasma Physics and Electrodynamics*, Academic, San Diego, Calif.

Kelley, M. C., B. G. Fejer, and C. A. Gonzales (1979), An explanation for anomalous ionospheric electric fields associated with a northward turning of the interplanetary magnetic field, *Geophys. Res. Lett.*, *6*(4), 301–304, doi:10.1029/GL006i004p00301.

Kelley, M. C., J. J. Makela, J. L. Chau, and M. J. Nicolls (2003), Penetration of the solar wind electric field into the magnetosphere/ionosphere system, *Geophys. Res. Lett.*, *30*(4), 1158, doi:10.1029/2002GL016321.

Kikuchi, T., and T. Araki (1979), Horizontal transmission of the polar electric field to the equator, *J. Atmos. Sol. Terr. Phys.*, *41*, 927–936, doi:10.1016/0021-9169(79)90094-1.

Kikuchi, T., H. Luhr, T. Kitamura, O. Saka, and K. Schlegel (1996), Direct penetration of the polar electric field to the equator during a DP2 event as detected by the auroral and equatorial magnetometer chains and the EISCAT radar, *J. Geophys. Res.*, *101*(A8), 17,161–17,173, doi:10.1029/96JA01299.

Kikuchi, T., K. K. Hashimoto, and K. Nozaki (2008), Penetration of magnetospheric electric fields to the equator during a geomagnetic storm, *J. Geophys. Res.*, *113*, A06214, doi:10.1029/2007JA012628.

Li, G., B. Ning, B. Zhao, L. Liu, W. Wan, F. Ding, J. S. Xu, J. Y. Liu, and K. Yumoto (2009), Characterizing the 10 November 2004 storm-time middle-latitude plasma bubble event in Southeast Asia using multi-instrument observations, *J. Geophys. Res.*, *114*, A07304, doi:10.1029/2009JA014057.

Li, G., et al. (2010), Longitudinal development of low-latitude ionospheric irregularities during the geomagnetic storms of July 2004, *J. Geophys. Res.*, *115*, A04304, doi:10.1029/2009JA014830.

Maruyama, N., et al. (2007), Modeling storm-time electrodynamics of the low-latitude ionosphere–thermosphere system: Can long lasting disturbance electric fields be accounted for?, *J. Atmos. Sol. Terr. Phys.*, *69*(10–11), 1182–1199, doi:10.1016/j.jastp.2006.08.020.

Nishida, A. (1968), Coherence of geomagnetic DP2 magnetic fluctuations with interplanetary magnetic variations, *J. Geophys. Res.*, *73*(17), 5549–5559, doi:10.1029/JA073i017p05549.

Richmond, A. D., and Y. Kamide (1988), Mapping electrodynamic features of the high-latitude ionosphere from localized observations: Technique, *J. Geophys. Res.*, *93*(A6), 5741–5759, doi:10.1029/JA093iA06p05741.

Ridley, A. J., and E. A. Kihn (2004), Polar cap index comparisons with AMIE cross polar cap potential, electric field, and polar cap area, *Geophys. Res. Lett.*, *31*, L07801, doi:10.1029/2003GL019113.

Ridley, A. J., G. Lu, C. R. Clauer, and V. O. Papitashvili (1998), A statistical study of the ionospheric convection response to changing interplanetary magnetic field conditions using the assimilative mapping of ionospheric electrodynamics technique, *J. Geophys. Res.*, *103*(A3), 4023–4039, doi:10.1029/97JA03328.

Sandel, B. R., et al. (2000), The extreme ultraviolet imager investigation for the IMAGE mission, *Space Sci. Rev.*, *91*, 197, doi:10.1023/A:1005263510820.

Sazykin, S. Y. (2000), Theoretical studies of penetration of magnetospheric electric fields to the ionosphere, Ph.D. thesis, Utah State Univ., Logan.

Spasojevic, M., and J. Goldstein (2005), Evidence of Effective Shielding in the Inner Magnetosphere?, *Eos Trans. AGU*, *86*(18), Jt. Assem. Suppl., Abstract SM42A-03.

Toffoletto, F., S. Sazykin, R. Spiro, and R. Wolf (2003), Inner magnetospheric modeling with the Rice Convection Model, *Space Sci. Rev.*, *107*, 175–196, doi:10.1023/A:1025532008047.

Tsyganenko, N. A., and D. P. Stern (1996), Modeling the global magnetic field the large-scale Birkeland current systems, *J. Geophys. Res.*, *101*(A12), 27,187–27,198, doi:10.1029/96JA02735.

Vasyliūnas, V. M. (2001), Electric field and plasma flow: What drives what?, *Geophys. Res. Lett.*, *28*(11), 2177–2180, doi:10.1029/2001GL013014.

Wei, Y., M. Hong, W. Wan, A. Du, J. Lei, B. Zhao, W. Wang, Z. Ren, and X. Yue (2008a), Unusually long lasting multiple penetration of interplanetary electric field to equatorial ionosphere under oscillating IMF Bz, *Geophys. Res. Lett.*, *35*, L02102, doi:10.1029/2007GL032305.

Wei, Y., M. Hong, W. Wan, A. Du, Z. Pu, M. F. Thomsen, Z. Ren, and G. D. Reeves (2008b), Coordinated observations of magnetospheric reconfiguration during an overshielding event, *Geophys. Res. Lett.*, *35*, L15109, doi:10.1029/2008GL033972.

Wei, Y., et al. (2009), Westward ionospheric electric field perturbations on the dayside associated with substorm processes, *J. Geophys. Res.*, *114*, A12209, doi:10.1029/2009JA014445.

Wei, Y., et al. (2010), Responses of the ionospheric electric field to the sheath region of ICME: A case study, *J. Atmos. Sol. Terr. Phys.*, doi:10.1016/j.jastp.2010.03.004, in press.

Weimer, D. R. (2001), Maps of ionospheric field-aligned currents as a function of the interplanetary magnetic field derived from Dynamics Explorer 2 data, *J. Geophys. Res.*, *106*, 12,889–12,902, doi:10.1029/2000JA000295.

Wolf, R. A., R. W. Spiro, S. Sazykin, and F. R. Toffoletto (2007), How the Earth's inner magnetosphere works: An evolving picture, *J. Atmos. Sol. Terr. Phys.*, *69*(3), 288–302, doi:10.1016/j.jastp.2006.07.026.

Xie, L., Z. Y. Pu, X. Z. Zhou, S. Y. Fu, and Q. G. Zong (2006), Energetic ion injection and formation of the storm-time symmetric ring current, *Ann. Geophys.*, *24*, 3547–3556, doi:10.5194/angeo-24-3547-2006.

Zong, Q.-G., B. W. Reinisch, P. Song, Y. Wei, and I. A. Galkin (2010), Dayside ionospheric response to the intense interplanetary shocks–solar wind discontinuities: Observations from the digisonde Global Ionospheric Radio Observatory, *J. Geophys. Res.*, *115*, A06304, doi:10.1029/2009JA014796.

J. Guo, State Key Laboratory of Space Weather (Center for Space Science and Applied Research, Chinese Academy of Sciences), Beijing 100190, China.

M. Hong, W. Wan, and Y. Wei, Beijing National Observatory of Space Environment, Institute of Geology and Geophysics, Chinese Academy of Sciences, Beijing 100012, China.

J. Liu, Polar Research Institute of China, Shanghai 200136, China.

Z. Pu and Q. Zong, School of Earth and Space Sciences, Peking University, 5 Yiheyuan St., Beijing 100871, China. (zypu@pku.edu.cn)

A. Ridley, Department of Atmospheric, Oceanic, and Space Sciences, University of Michigan, Ann Arbor, MI 48109-2143, USA.